ELSEVIER

Journal of Magnetism and Magnetic Materials 223 (2001) 284–292

Journal of magnetism and magnetic materials

www.elsevier.com/locate/jmmm

Biquadratic exchange coupling in an unequal Fe/Cr/Fe(1 0 0) trilayer

P. Vavassori[a,1], M. Grimsditch[a,*], Eric E. Fullerton[b]

[a]*Materials Science Division 223, Argonne National Laboratory, 9700 S. Cass Ave., Argonne, IL 60439, USA*
[b]*IBM, Almaden Research Center, San Jose, CA 95120-6099, USA*

Received 14 July 2000; received in revised form 1 November 2000

Abstract

We have investigated the magnetic properties of a (1 0 0)-oriented unequal trilayer, Fe(45 Å)/Cr(30 Å)/Fe(15 Å), by means of Brillouin light scattering and magnetization measurements. The experimental results show that this sample highlights the effect of biquadratic coupling which aligns the magnetization of the Fe layers at 90° to each other. We extracted the bilinear and biquadratic coupling strengths by fitting the experimental results with a theory that treats the static and dynamic responses on an equal footing. Our results confirm that the model describes both the static and dynamic properties even when the magnetization of the layers is aligned at 90°. The coupling strengths, and their temperature dependence, are discussed and compared with other results reported in the literature.

Keywords: Fe/Cr superlattices; Magnetic; Biquadratic; Bilinear; Brillouin scattering; And MOKE

1. Introduction

Fe/Cr/Fe(1 0 0) trilayer structures were the first systems in which indirect exchange coupling across a nonmagnetic transition-metal spacer layer was observed [1] along with its oscillatory dependence on interlayer thickness [2]. The leading term of the coupling is a Heisenberg-like bilinear term that results in parallel or antiparallel alignment of adjacent Fe layers. The presence of an additional biquadratic coupling term $(s_1 \cdot s_2)^2$ is now also well established; this coupling favors 90° alignment of adjacent layers and has been discussed in a number of recent reviews [3–5]. The oscillatory bilinear coupling has two periods for Cr spacer layers; a long (18 Å) period and, for atomically smooth surfaces, a two-monolayer period that can be directly related to the antiferromagnetic properties of Cr. Both periods can be related to the Cr Fermi surface, the short period results from the nested Fermi surface and the long period from the N-centered ellipse [6,7].

* Corresponding author. Tel.: + 1-630-252-5544; fax: + 1-630-252-7777.
E-mail address: grimsditch@anl.gov (M. Grimsditch).
[1] Present address: INFM-Dipartamento di Fisica, Universitá de Ferrara, via Paradiso 12, I-44100 Ferrara.

0304-8853/01/$ - see front matter
PII: S0304-8853(00)01334-2

Although the period of the coupling is quantitatively understood, the strength and phase of the oscillatory coupling is less well understood and is found to depend on both the roughness and interdiffusion at the Fe–Cr interfaces. For a recent review, see Pierce et al. [7].

Biquadratic coupling often exhibits a stronger temperature dependence than the bilinear coupling. Although biquadratic coupling can, in principle, be an intrinsic property of indirect exchange coupling [8–11] it is now thought to mostly arise from a variety of extrinsic mechanisms. Several mechanisms have been suggested to explain this behavior as arising from structural imperfections that average over varying bilinear contributions and result in a biquadratic term. As summarized in Ref. [4] they are the fluctuation mechanism [12], loose spin model [13], and the magnetic–dipole model [14]. For Cr interlayers, its intrinsic antiferromagnetic order is also thought to contribute to the biquadratic coupling [3–7,15–19]. This is supported for thicker Cr layers ($t_{Cr} > 42$ Å) by the experimental results which show that for Fe/Cr samples, a strong correlation exists between magnetic phase transitions in the antiferromagnetic Cr layers and the biquadratic coupling [17,18]. For thinner Cr layers, the relation between the antiferromagnetic order within the Cr interlayer and biquadratic coupling is less clear but correlations between non-collinear alignment of the Fe layers and Cr antiferromagnetism have been observed by Schreyer et al. [19]. This behavior is probably related to Slonczewski's proximity magnetism model [3]. Clearly, a deeper understanding of biquadratic coupling in this and related systems requires careful measurements of the interlayer exchange terms.

In this paper we use an experimental approach for determining these coefficients based on the fitting of BLS and magnetization measurements. This approach, successfully used in recent investigations [5,15,20–23], is here applied to an Fe(45 Å)/Cr(30 Å)/Fe(15 Å) trilayer in which the two magnetic layers have different thicknesses. The thickness of the Cr interlayer was chosen in order to highlight the effects of biquadratic coupling. As will be shown, at certain fields the two magnetic layers are aligned at 90° and provide an opportunity to investigate the magnetic excitations in such a configuration and to test the models which are used to interpret the BLS spectra [23]. The values obtained for the coupling strengths and their temperature dependence are discussed and compared with other results reported in the literature.

2. Experimental details

The sample was epitaxially grown by DC magnetron sputtering on a polished single-crystal MgO(1 0 0) substrate using the same procedure outlined for superlattices [24]. A 100 Å Cr(1 0 0) layer was grown at 600°C. The substrate was then cooled to ≈ 75°C prior to the growth of the Fe(45 Å)/Cr(30 Å)/Fe(15 Å) trilayer. The complete structure was then capped with a 30 Å Cr layer. A calibrated quartz crystal oscillator monitored the thickness of the various layers. Under these conditions, the layers grow along a [1 0 0] direction and exhibit a four-fold in-plane anisotropy with the easy axes along the remaining $\langle 1\,0\,0 \rangle$ directions.

The magnetization hysteresis loops were measured by SQUID magnetometry. The spin-wave excitations were measured by BLS using 250 mW of 5145 Å radiation from an Ar^+ laser. The scattered radiation was analyzed with a tandem Fabry–Perot interferometer [25] in 3 + 2 pass operation. The sample was mounted with its normal along the collection axis and the laser beam was incident at an angle of 50° to the normal. This geometry fixes the magnitude of the wave vector parallel to the surface $q_{\parallel}$ at $0.93 \times 10^5\,cm^{-1}$. The magnetic field was applied in the plane of the sample and perpendicular to the scattering plane, i.e. perpendicular to the wave vector of the magnon. The sample could be rotated about the normal, thereby allowing the magnetic field to be applied along different in-plane directions. The polarization of the scattered light was analyzed at 90° to the incident polarization in order to minimize the intense signal of the unshifted laser radiation. All BLS measurements were made at room temperature.

3. Results and discussion

Fig. 1 shows the room temperature magnetization results of our sample when H is applied along the in-plane easy-axis of the sample. The magnetization curve in the low-field region (0–100 Oe) is characterized by a square hysteresis loop centered at $H = 0$ and with a partial saturation value for M, that is a half of the saturation value M_s at higher fields. The qualitative interpretation of this portion of the loop shows that the AF coupling is dominant and the magnetization of the two Fe layers are antiparallel, lie in the film plane, and are along the easy axis. The value of $M = 0.5\ M_s$ is consistent with the different thicknesses of the two films, i.e. $M/M_s = (d_2 - d_1)/(d_1 + d_2) = 0.5$ for our sample with $d_1 = 15$ Å and $d_2 = 45$ Å. This assumes the same value for the saturation magnetization in the two films. As the field increases two first-order phase transitions are observed. The first occurring at $H \approx 100$ Oe is consistent with the spins switching from being antiparallel to a situation in which M for the thinner layer is oriented along the other easy axis and is almost at 90° to the field and to the other (thick) layer. In this region $M/M_s = d_2/(d_1 + d_2) = \frac{3}{4}$ as expected. The second transition takes place at $H \approx 260$ Oe and corresponds to parallel alignment of the spins along the field direction. The above qualitative behavior indicates that the spins are at 90° to each other over the range 100–260 Oe. Our purpose is to determine the numerical strengths of the anisotropies and biaxial and bilinear coupling which stabilize this configuration.

Our aim is also to ensure that the model that accounts for the magnetization, is also capable of describing the BLS frequencies. As expected for two magnetic layers of these thicknesses, the BLS spectra show two modes which can be viewed as the in-phase (symmetric mode) and out-phase (antisymmetric mode) oscillations of the two Fe layers. The frequencies of the symmetric and antisymmetric modes as a function of the external field H are shown in Fig. 2, for H applied along the easy axis and in Fig. 3 for H along the hard axis. Blow-ups of the frequencies in the 0–1 kOe range are shown in Fig. 4 for both field orientations.

The numerical values of the magnetic parameters have been obtained by fitting the field dependence of the magnetization and BLS results. The basics of the model are described in Ref. [23]; a slightly modified version of that approach was used in Ref. [20]. Our approach here follows that in Ref. [20] but includes the obvious changes necessary to account for the two layers having different thicknesses. At any given field the minimum of the total energy with respect to the orientation of the magnetization yields the equilibrium magnetic configuration from which the magnetization can be calculated and compared with the SQUID results. The

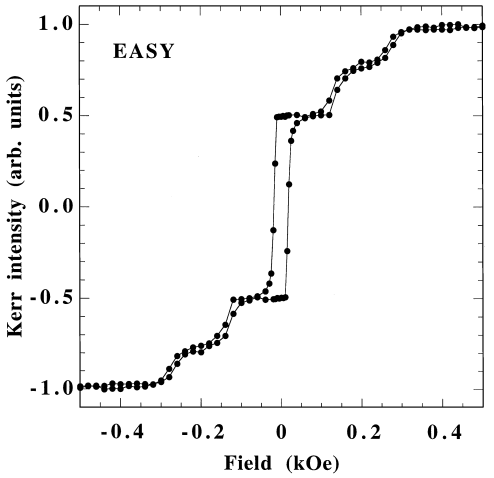

Fig. 1. SQUID loop measured with the field applied along the easy axis. The full line is a guide to the eye.

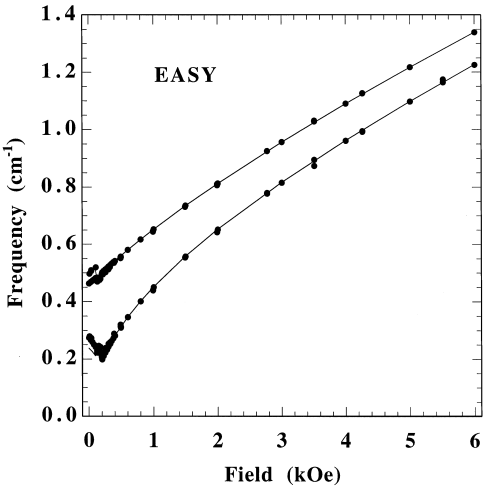

Fig. 2. Brillouin frequencies as a function of the external field applied along the easy axis: experiment (dots) and fit (line) described in the text.

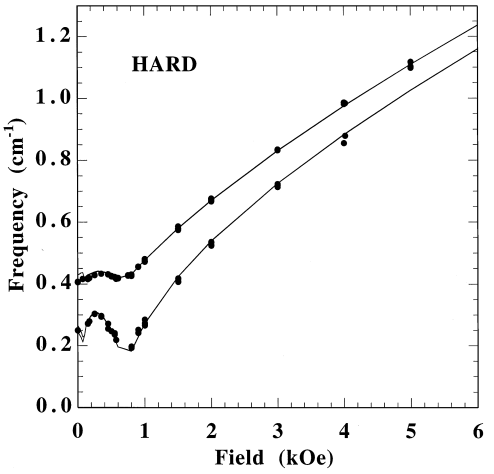

Fig. 3. Brillouin frequencies as a function of the external field applied along the hard axis: experiment (dots) and fit (line) described in the text.

magnon frequencies, obtained as perturbations of the layers from their equilibrium state, are then compared with the BLS results.

The total energy per unit area is given by the sum of anisotropy, Zeeman and coupling terms

$$\begin{aligned} E &= E_a + E_z + E_{in} \\ &= K_1 d_1 \sin^2(2\theta_1) + K_2 d_2 \sin^2(2\theta_2) - M_1 d_1 H \cos(\theta_1 - \theta_H) - M_2 d_2 H \cos(\theta_2 - \theta_H) \\ &\quad + J_1 \cos(\theta_1 - \theta_2) + J_2 \cos^2(\theta_1 - \theta_2), \end{aligned} \tag{1}$$

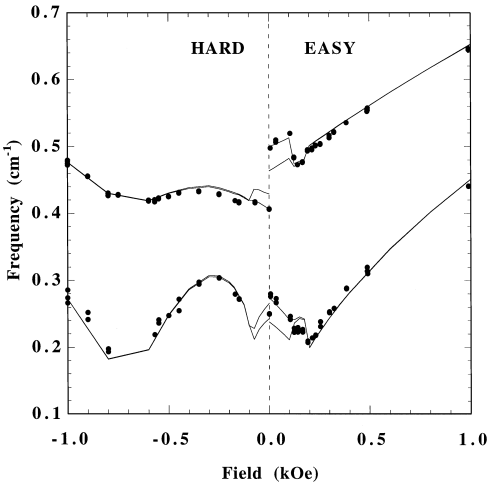

Fig. 4. Blow-up of Figs. 2 and 3 in the region 0–1 kOe. For clarity the hard-axis results have been plotted along negative field axis.

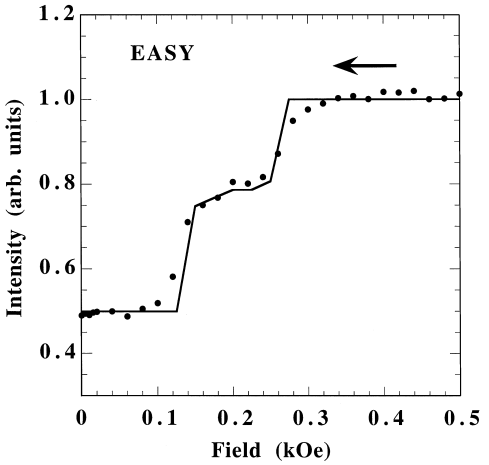

Fig. 5. Fit (full line) to magnetization data in Fig. 1.

where K_1 and K_2 are the cubic anisotropy constants of the two magnetic layers, M_1 and M_2 their magnetization, H is the applied field, J_1 and J_2 are the bilinear and biquadratic coupling constants and θ_1, θ_2 and θ_H the angles that the magnetization and applied field subtend with the easy axis. H along the easy and hard axes corresponds to $\theta_H = 0$ and $\pi/4$, respectively.

In order to extract the material parameters we minimize the energy expression for given (numerical) values of K_1, K_2, M_1, M_2, J_1, J_2 and H to determine θ_1 and θ_2. The easy-axis magnetization is then given by $(M_s d_1 \cos\theta_1 + M_2 d_2 \cos\theta_2)/(M_s d_1 + M_2 d_2)$. Fig. 5 shows our best fit of the magnetization loop. The best fit parameters are listed in Table 1, where an asterisk indicates that the fit was insensitive to that particular parameter. Therefore, during the fitting of the SQUID results we have fixed the values of the cubic anisotropy constants (K_1 and K_2) and of the saturation magnetization in the two films (M_1 and M_2) to the values extracted from the fits to the BLS data.

Table 1
Parameters extracted from the best least-squares fitting of the data shown in Figs. 1–4[a]

	$K_a(\times 10^5\,\mathrm{ergs\,cm^{-3}})$	$K_b(\times 10^5\,\mathrm{ergs\,cm^{-3}})$	$4\pi M_a$(kG)	$4\pi M_b$(kG)	$J_1(\times 10^{-2}\,\mathrm{ergs\,cm^{-2}})$	$J_2(\times 10^{-2}\,\mathrm{ergs\,cm^{-2}})$
BLS	1.9 ± 0.6	4.5 ± 0.8	20.2 ± 1.3	20.7 ± 1.2	3.85 ± 1.35	0.75 ± 0.55
SQUID	1.9*	4.5*	20.2*	20.7*	4.70 ± 0.20	1.35 ± 0.25

[a] K are cubic anisotropies, $4\pi M$ are effective magnetizations (which may include contributions from the perpendicular anisotropy as described in the text), and J_1 and J_2 are the inter-layer bilinear and biquadratic coupling strengths, respectively. Subscripts a and b indicate properties of the 15 and 45 Å Fe layers, respectively. Also shown are confidence levels obtained as described in the text.

The formalism we use to derive the magnon frequencies is conceptually the same as that used in Ref. [20]. We stress that, since in this formalism the same energy expression yields both the magnetization and the magnon frequencies, it guarantees that any discrepancies between BLS and magnetization results cannot be attributed to inconsistent forms of the energy expression. In the present case, differences produced by considering layers with different thicknesses and magnetizations require changes to matrices $A5$ and $A6$ of Ref. [20]. (Note that in Eq. (1) we have omitted the out of plane dependence for simplicity, the generalizations to include it are straightforward following [20].) With the notation that $E_{\alpha\beta}$ are the second derivatives of the energy with respect to the variables α and β, these matrices are now

$$\begin{vmatrix} E_{\theta_1\theta_1}/d_1 & E_{\theta_1\phi_1}/d_1 - i\omega M_1 & E_{\theta_1\theta_2}/d_2 & E_{\theta_1\phi_2}/d_2 \\ E_{\phi_1\theta_1}/d_1 + i\omega M_1 & E_{\phi_1\phi_1}/d_1 & E_{\phi_1\theta_2}/d_2 & E_{\phi_1\phi_2}/d_2 \\ E_{\theta_2\theta_1}/d_1 & E_{\theta_2\phi_1}/d_1 & E_{\theta_2\theta_2}/d_2 & E_{\theta_2\phi_2}/d_2 - i\omega M_2 \\ E_{\phi_2\theta_1}/d_1 & E_{\phi_2\phi_1}/d_1 & E_{\phi_2\theta_2}/d_2 + i\omega M_2 & E_{\phi_2\phi_2}/d_2 \end{vmatrix}. \tag{2}$$

and

$$2\pi q_{\parallel} \begin{vmatrix} \cos^2(\theta_1-\theta_h)d_1M_1^2 & 0 & \cos(\theta_1-\theta_h)\cos(\theta_2-\theta_h)d_1M_1M_2 & i\cos(\theta_1-\theta_h)d_1M_1M_2 \\ 0 & -d_1M_1^2 & i\cos(\theta_2-\theta_h)d_1M_1M_2 & d_1M_1M_2 \\ \cos(\theta_1-\theta_h)\cos(\theta_2-\theta_h)d_2M_1M_2 & -i\cos(\theta_2-\theta_h)d_2M_1M_2 & \cos^2(\theta_2-\theta_h)d_2M_2^2 & 0 \\ -i\cos(\theta_1-\theta_h)d_2M_1M_2 & -d_2M_1M_2 & 0 & -d_2M_2^2 \end{vmatrix}. \tag{3}$$

The magnon frequencies are obtained by solving the secular equation of the sum of these two matrices. In analyzing the BLS data we found that simultaneously fitting the easy- and hard-axis data considerably reduced the uncertainties. The results of the fitting are shown by the full lines in Figs. 2 and 3 over the whole field range while Fig. 4 shows them in more detail in the range 0–1 kOe in which the spin–flop first-order phase transitions take place. The agreement between the experimental data and the fits is excellent since the modeling accounts for even small details at low fields. The splitting, observed in the calculations at low fields, occurs in the regions where the Stokes and the anti-Stokes portions of the spectra are not time reversal invariant of each other. For larger fields, where the two layers are aligned with the field, no such differences exist. All the curves presented in Figs. 2–4 correspond to least-squares fits to the data and the best fit values for the material parameters are listed in Table 1.

3.1. Determination of errors

In our least-squares fitting χ^2, the sum of the square of the differences between calculation and experiment, is evaluated and the parameters varied to find its minimum value. The error estimate for each parameter, which is described in detail in Ref. [20], involves finding the change such that the χ^2 after adjusting all other parameters increases by 50%.

Crucial in the comparison of the results extracted from magnetization and BLS summarized in Table 1 are the estimated uncertainties. Because the values extracted for J_1 and J_2 are within the estimated errors, we can claim that the energy given by Eq. (1) provides a self-consistent description of the experimental results. Although this may seem somewhat trivial, we note that since J_2 is introduced into the theory on purely phenomenological grounds, it is not a priori obvious that it will describe all physical properties correctly. In this context it validates the postulate that there is an interaction between magnetic layers, which favors 90° alignment. The approach of independently fitting the results of several experimental measurements has the additional advantage of yielding more reliable estimates of the coupling parameters and their confidence levels.

The value of $4.5 \times 10^5\,\mathrm{ergs\,cm^{-3}}$ found for K_2 is close to the bulk value and in good agreement with the reported values for 40 Å Fe layer [22]. The value of K_1 is smaller than K_2, as expected for a thinner layer and it is close to that reported in Ref. [20] for similar Fe thicknesses. The magnetization values of both films are slightly smaller than for bulk Fe and are consistent with previous determinations [20,22,26–29]. Part of the reduction may be due to the fact that BLS is sensitive to $4\pi M_{\mathrm{eff}} = 4\pi M - 2K_{\mathrm{perp}}/M$, where the perpendicular anisotropy is typically induced by the surface.

Returning to the values for J_1 and J_2 we observe that the values determined from BLS are smaller than those obtained from SQUID measurements but that they have larger error bars. The larger error bars in the BLS results are related to the larger number of fitting parameters, which allow for a greater degree of interdependence. On the other hand, the SQUID measurements, being sensitive only to the interlayer coupling parameters, produce noticeably smaller error bars. Particularly relevant is the relatively small uncertainty in the value of the biquadratic exchange parameter J_2 that is often determined with large uncertainties since it is difficult to separate from the usually large J_1 contribution. The accuracy of the present determination is due to two reasons: (i) the reduction of the bilinear coupling interaction through the appropriate choice of the Cr interlayer thickness; (ii) the inequality of the two Fe layer thicknesses. Both these conditions contribute to make the magnetization jumps more evident in the first-order spin flop transitions.

There is only one other determination of J_1 and J_2 for the (1 0 0) orientation and the same Cr thickness [21]. In units of $10^{-2}\,\mathrm{ergs\,cm^{-2}}$ our $J_1 = 4.7 \pm 0.2$ and $J_2 = 1.35 \pm 0.25$ do not agree well with 0.4 and 0.22 from Ref. [21]. The agreement is somewhat better when compared with measurements on an Fe/Cr/Fe(1 0 0) trilayer with a 25 Å Cr layer that gave $2.4 \times 10^{-2}\,\mathrm{ergs\,cm^{-2}}$ for both J_1 and J_2 [22]. Discrepancies in measured values of the coupling strengths are common and are typically ascribed to the microscopic differences in the sample characteristics. Since these effects have been extensively discussed [7,15], we will not pursue this issue further.

Given the difficulty in interpreting absolute values of the coupling strengths, it is interesting to consider their temperature dependence to probe the origin of the coupling. In recent studies of FeSi/Fe superlattices [30,31] it was suggested (based on the authors' interpretation of the quantum interference model of Bruno [32]) that the observed temperature dependence of J_1 and J_2 could be explained by

$$J_1 = J_1^0(T/T_0)/\sinh(T/T_0),$$
$$J_2 = J_2^0(2T/T_0)/\sinh(2T/T_0), \tag{4}$$

where the superscript 0 indicates the value at 0 K and T_0 is a function of the spacer layer properties and is expected to scale as the inverse of the layer thickness. In Fig. 6 we have plotted the coupling strengths,

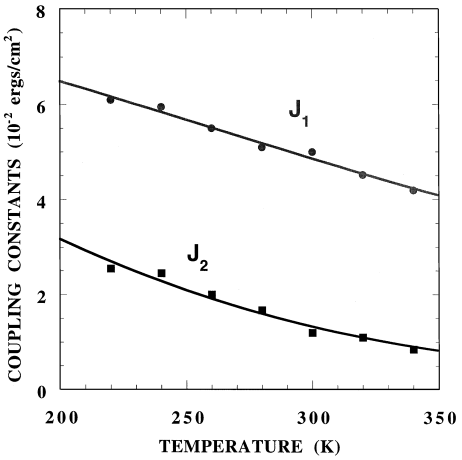

Fig. 6. Temperature dependence of J_1 and J_2 obtained from magnetization. The full lines are the fit according to Eqs. (4).

obtained from magnetization loops, as a function of temperature. The full lines are fits to Eq. (4) with, $J_1^0 = 8.4 \times 10^{-2}\,\mathrm{ergs\,cm^{-2}}$, $J_2^0 = 7.9\ 10^{-2}\,\mathrm{ergs\,cm^{-2}}$ and $T_{0_2} = 158\,\mathrm{K}$. A similar fit to the temperature dependence of J_1 was reported in Ref. [33]; for 11, 13 and 15 Å Cr thicknesses they obtained $T_0 = 390$, 214 and 122 K, respectively. We have also fitted the temperature dependence of the results presented in Ref. [34] for a 16 Å Cr layer and obtained $T_0 = 144\,\mathrm{K}$. Hence, even though the functional form given by Eq. (4) seems to describe the measured temperature dependence of J_1 and J_2, the values obtained for T_0 do not scale as the inverse of thickness as predicted by the equations given in Ref. [30].

4. Conclusions

In this study we determined the coupling coefficients in a (1 0 0)-oriented unequal trilayer Fe(45 Å)/Cr(30 Å)/Fe(15 Å) in which the thickness of the Cr interlayer was chosen in order to highlight the effects of biquadratic coupling. To evaluate the coefficients, we use an experimental approach based on the fitting of the BLS and magnetization measurements. We obtained consistent values of the magnetic parameters by fitting the experimental results with a theory treating the static and dynamic responses on an equal footing. Our results confirm the theoretical model used in interpreting both the static and dynamic properties even in systems in which the magnetization of the layers is aligned at 90°.

As found in previous investigations, the values obtained for the bilinear and biquadratic coupling strengths are not in perfect agreement with previous results reported in the literature for the same Cr spacer thickness. This has been interpreted as being due to the details of the interfaces at the atomic level. We also find that the temperature dependence of the coupling strengths, although they can be fitted by the equations proposed by Endo et al. [30], produce fitting parameters that do not scale according to the predictions of that theory.

Acknowledgements

Work at Argonne National Laboratory was supported by the US Department of Energy, Division of Material Sciences, Office of Basic Energy Sciences, under contract W-31-109-ENG-38. We thank

C.H. Sowers for the Fe film deposition. P.V. acknowledges support by a research grant from INFM-Istituto Nazionale per la Fisica della Materia.

References

[1] P. Grünberg, R. Schreiber, Y. Pang, M.D. Brodsky, H. Sowers, Phys. Rev. Lett. 57 (1986) 2442.
[2] S.S. Parkin, N. More, K.P. Roche, Phys. Rev. Lett. 64 (1990) 2304.
[3] J.C. Slonczewski, J. Magn. Magn. Mater. 150 (1995) 13.
[4] S.O. Demokritov, J. Phys. D: Appl. Phys. 31 (1998) 925.
[5] B. Heinrich, J.F. Cochran, Adv. Phys. 42 (1993) 523.
[6] M.D. Stiles, J. Magn. Magn. Mater. 200 (1999) 322.
[7] D.T. Pierce, J. Unguris, R.J. Celotta, M.D. Stiles, J. Magn. Magn. Mater. 200 (1999) 290.
[8] R.P. Erickson, K.B. Hathaway, J.R. Cullen, Phys. Rev. B 47 (1993) 2626.
[9] J. Barnas, P. Grünberg, J. Magn. Magn. Mater. 121 (1993) 326.
[10] J. Barnas, J. Magn. Magn. Mater. 123 (1993) L21.
[11] D.M. Edwards, J.M. Ward, J. Mathon, J. Magn. Magn. Mater. 126 (1993) 380.
[12] J.C. Slonczewski, Phys. Rev. Lett. 67 (1991) 3172.
[13] J.C. Slonczewski, J. Appl. Phys. 73 (1993) 5957.
[14] S. Demokritov, E. Tsymbal, P. Grünberg, W. Zinn, I.K. Schuller, Phys. Rev. B 49 (1994) 720.
[15] B. Heinrich, J.F. Cochran, T. Monchesky, R. Urban. Phys. Rev. B 59 (1999) 14520.
[16] H. Zabel, J. Phys.: Condens. Matter 11 (1999) 9303.
[17] E.E. Fullerton, K.T. Riggs, C.H. Sowers, S.D. Berger, A. Berger, Phys. Rev. Lett. 75 (1995) 330.
[18] E.E. Fullerton, S.D. Bader, J.L. Robertson, Phys. Rev. Lett. 77 (1996) 1382.
[19] A. Schreyer, C.F. Majkrzak, T. Zeidler, T. Schmitte, P. Bodeker, K. Theis-Brohl, A. Abromeit, J.A. Dura, T. Watanabe, Phys. Rev. Lett. 79 (1997) 4914.
[20] M. Grimsditch, S. Kumar, E.E. Fullerton, Phys. Rev. B 54 (1996) 3385.
[21] R.J. Hicken, C. Daboo, M. Gester, A.J.R. Ives, S.J. Gray, J.A.C. Bland, J. Appl. Phys. 78 (1995) 6670.
[22] S.M. Rezende, C. Chesman, M.A. Lucena, A. Azevedo, F.M. Aguiar, S.S.P. Parkin, J. Appl. Phys. 84 (1998) 958.
[23] J.F. Cochran, J. Rudd, W.B. Muir, B. Heinrich, Z. Celinski, Phys. Rev. B 42 (1990) 508.
[24] E.E. Fullerton, M.J. Conover, J.E. Mattson, C.H. Sowers, S.D. Bader, Phys. Rev. B 48 (1993) 15755.
[25] J.R. Sandercock, in: M. Cardona, Güntherodt (Eds.), Light Scattering in Solids III, Springer, Berlin, 1982, p. 173.
[26] R. Kabos, C.E. Patton, M.O. Dima, D.B. Church, R.L. Stamps, R.E. Camley, J. Appl. Phys. 75 (1994) 3553.
[27] C. Chesman, M.A. Lucena, M.C. de Moura, A. Azevedo, F.M. deAguiar, S.M. Rezende, S.S.P. Parkin, Phys. Rev. B 58 (1998) 101.
[28] A. Azevedo, C. Chesman, M.A. Lucena, F.M. deAguiar, S.M. Rezende, S.S.P. Parkin, J. Magn. Magn. Mater. 177–181 (1998) 1177.
[29] A. Azevedo, C. Chesman, S.M. Rezende, F.M. deAguiar, X. Bian, S.S.P. Parkin, Phys. Rev. Lett. 76 (1996) 4837.
[30] Y. Endo, O. Kitakami, Y. Shimada, Phys. Rev. B 59 (1999) 4279.
[31] G.J. Strijkers, J.T. Kohlhepp, H. Swagten, W. de Jonge, Phys. Rev. Lett. 84 (2000) 1812.
[32] P. Bruno, J. Appl. Phys. 76 (1994) 6972.
[33] S.M. Rezende, C. Chesman, M.A. Lucena, M.C. de Moura, A. Azevedo, F.M. de Aguiar, S. Parkin, J. Appl. Phys. 85 (1999) 5892.
[34] M. Fromn, L.X. Liao, J.F. Cochran, B. Heinrich, J. Appl. Phys. 75 (1994) 6181.